07 Apr 2015

Slip Length Crossover on a Graphene Surface

Zhi Liang
Missouri University of Science and Technology, zlch5@mst.edu

Pawel Keblinski

Recommended Citation

Z. Liang and P. Keblinski, "Slip Length Crossover on a Graphene Surface," *Journal of Chemical Physics*, vol. 142, no. 13, article no. 134701, American Institute of Physics, Apr 2015.
The definitive version is available at https://doi.org/10.1063/1.4916640

The Journal of Chemical Physics

Slip length crossover on a graphene surface

Cite as: J. Chem. Phys. **142**, 134701 (2015); https://doi.org/10.1063/1.4916640
Submitted: 16 February 2015 • Accepted: 19 March 2015 • Published Online: 01 April 2015

Zhi Liang and Pawel Keblinski

AIP Publishing

Slip length crossover on a graphene surface

Zhi Liang[1,a)] and Pawel Keblinski[1,2,b)]
[1]*Rensselaer Nanotechnology Center, Rensselaer Polytechnic Institute, Troy, New York 12180, USA*
[2]*Department of Materials Science and Engineering, Rensselaer Polytechnic Institute, Troy, New York 12180, USA*

(Received 16 February 2015; accepted 19 March 2015; published online 1 April 2015)

Using equilibrium and non-equilibrium molecular dynamics simulations, we study the flow of argon fluid above the critical temperature in a planar nanochannel delimited by graphene walls. We observe that, as a function of pressure, the slip length first decreases due to the decreasing mean free path of gas molecules, reaches the minimum value when the pressure is close to the critical pressure, and then increases with further increase in pressure. We demonstrate that the slip length increase at high pressures is due to the fact that the viscosity of fluid increases much faster with pressure than the friction coefficient between the fluid and the graphene. This behavior is clearly exhibited in the case of graphene due to a very smooth potential landscape originating from a very high atomic density of graphene planes. By contrast, on surfaces with lower atomic density, such as an (100) Au surface, the slip length for high fluid pressures is essentially zero, regardless of the nature of interaction between fluid and the solid wall. © *2015 AIP Publishing LLC.* [http://dx.doi.org/10.1063/1.4916640]

I. INTRODUCTION

Due to a high atomic surface density and high contact angle, fluid flow on a graphene surface is characterized by a high slip length.[1–3] A large slip length is favorable for the pressure-driven transport of fluid in nanochannels and can significantly enhance the efficiency of many nanofluidic applications such as electrokinetic energy conversion in nanofluidic channels.[2] The slip length of various liquids, such as water and liquid Ar, on graphene has been investigated by numerous experiments and simulations.[3–9] Generally, a large slip length in the range from ∼10 nm to ∼100 nm was found in both experiments and simulations.

Kinetic theory predicts that the slip length of gases on graphene (or any other surface for that matter) is proportional to the molecular collision mean free path (MFP), which decreases with increasing pressure.[10] Accordingly, the slip length of a gas on graphene also decreases with increasing pressure. Consequently, at high pressures, the MFP and the slip length of gases could be as small as a nanometer. This value is much smaller than that characterizing liquid flow on graphene. This suggests that as a function of increasing pressure, when the fluid transitions from the gas to liquid-like behavior, there is a minimum slip length. However, molecular dynamics (MD) simulations of the pressure dependence of the fluid slip on the Au surface show that the slip length generally decreases with increasing pressure and does not exhibit a minimum.[11] To elucidate this contradiction, we carry out equilibrium MD (EMD) and non-equilibrium MD (NEMD) simulations of Ar flow at various pressures in graphene nanochannels.

a)Electronic mail: liangz3@rpi.edu
b)Electronic mail: keplip@rpi.edu

II. PRESSURE-DEPENDENT SLIP LENGTH ON GRAPHENE

A. The MD model

The model system consists of a graphene nanochannel filled with fluid Ar (see Fig. 1(a)). Each solid wall contains three graphene atomic planes. The cross section area, A, of the model system is $L_x = 5.23$ nm by $L_y = 5.23$ nm, and the distance between the two innermost graphene layers is $L_z = 10$ nm. The periodic boundary conditions (PBCs) are applied at x and y directions, and the atomic position in the outer graphene planes is fixed. We model the C-C interactions within graphene planes with the optimized Tersoff potential.[12] The Lennard-Jones (LJ) potential, with parameters $\sigma_{c\text{-}c} = 3.41$ Å and $\varepsilon_{c\text{-}c} = 2.39$ meV,[13] is applied between carbon atoms belonging to the different graphene planes. The LJ potential is also employed for Ar-Ar interactions with parameters $\sigma_{Ar\text{-}Ar} = 3.41$ Å and $\varepsilon_{Ar\text{-}Ar} = 10.3$ meV,[14] and for Ar-carbon interactions with parameters determined by the Lorentz-Berthelot mixing rule. The cutoff distance is $2.5\sigma_{Ar\text{-}Ar}$ for all LJ interactions. In all MD simulations, we use a velocity Verlet algorithm with multiple time step sizes for the integration of the equations of motions.[15] A time step of 0.5 fs is used for in-plane carbon-carbon interactions, and 5 fs is used for all other interactions. To investigate how the slip length on graphene varies with pressure, we gradually change the density of fluid Ar in the graphene nanochannel. All simulations are performed at a temperature of 150 K, which is above the critical temperature to avoid complications associated with the coexistence of two (liquid and vapor) phases in the nanochannel.

B. The critical temperature and pressure

For reference, we determined the critical temperature and pressure, T_{cr} and P_{cr}, of the model bulk fluid Ar. The simulation

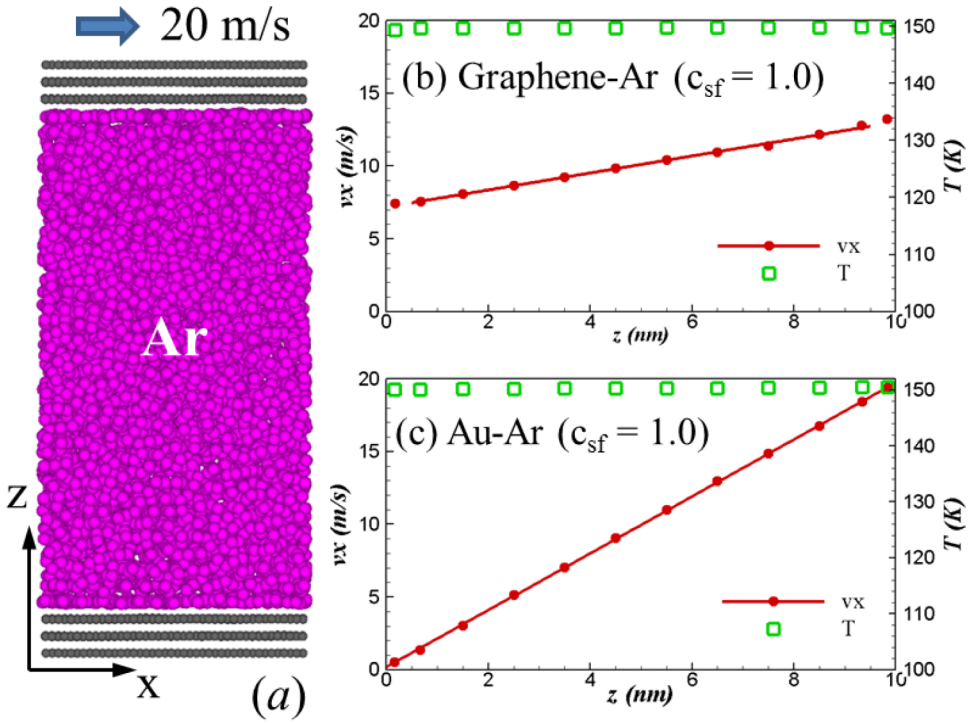

FIG. 1. (a) A snapshot of fluid Ar in a graphene nanochannel. Velocity and temperature distributions of fluid Ar in (b) a graphene channel and (c) a Au channel at 150 K and 955 atm.

detail is described in our previous work.[16] Briefly, we placed a liquid slab of 2160 Ar atoms in the middle of a simulation box which has a length of 19.2 nm and cross section area of 3.84 nm × 3.84 nm. The box size is fixed during the simulation, and PBCs are applied in all three directions. We equilibrated the system at multiple temperatures varying from 85 K to 150 K using the Berendsen thermostat.[17] Below T_{cr}, the liquid and vapor phases were both present in the same simulation cell. Fig. 2 shows the density of saturated vapor and liquid as a function of temperature. From the simulation, we find T_{cr} = 132 K and P_{cr} = 44 atm.

C. NEMD determination of slip length on graphene

Now, we turn to the NEMD simulation of Couette flow between two graphene surfaces. The atomic density of fluid

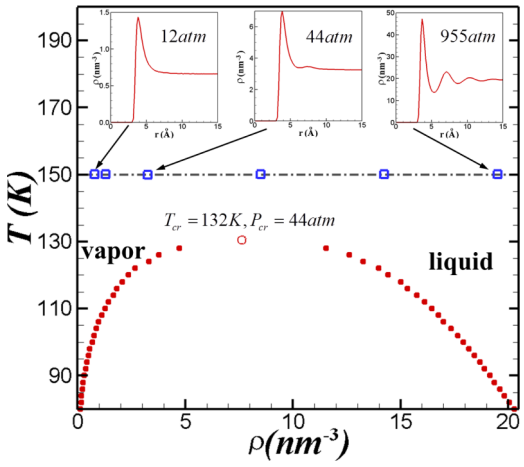

FIG. 2. The T vs. ρ phase diagram of bulk fluid Ar. The red dots show the density of saturated vapor and saturated liquid at a given temperature. The blue squares show the thermodynamic states of Ar in the simulation. The insets are the RDF of fluid at different thermodynamic states.

Ar (as determined at the center of the nanochannel) is varied from 0.66/nm^3 to 19.8/nm^3, with the six simulated state points of fluid indicated in Fig. 2 (density at the critical point is ~7.6/nm^3). To generate a Couette flow, the upper graphene wall is moved in the x-direction at 20 m/s while the lower wall is fixed. To avoid the artifacts associated with freezing wall atoms and thermostating the fluid,[3,6] the Berendsen thermostat[17] is applied to the center graphene plane in each wall to maintain the system at 150 K. For statistical averaging, the fluid region is evenly divided into 10 bins in the z-direction to monitor temperature and velocity. In all NEMD simulations, 10 ns is used to allow the system to reach a steady state, and then 80 ns is used for data collection and averaging. The fluid pressure is determined by F_p/A, where F_p is the average pressure force acting on the graphene surface by fluid.

The typical temperature and velocity profile for fluid flow at 955 atm (the highest pressure in our simulation) is shown in Fig. 1(b). The linear fit to the velocity data points gives slip lengths on the top and bottom surfaces and an average slip length of 11.9 ± 0.2 nm. The uncertainty is obtained by analysis of four independent runs. It is also shown in Fig. 1(b) that the fluid temperature is essentially a constant across the channel. To ensure that the NEMD simulation is in the linear response regime, we reduced the velocity of the upper wall to 10 m/s and we obtained essentially same slip length.

The slip length as a function of pressure is shown in Fig. 3(a). According to Fig. 3(a), the minimum slip length of 1.5 ± 0.3 nm is obtained at 44.5 atm which is very close to P_{cr} = 44 atm. The radial distribution function (RDF) of a bulk fluid at 150 K and 44 atm is shown in Fig. 2. This RDF exhibits an onset of a second peak, which indicates a transition from the vapor state to the supercritical fluid (structurally liquid-like) state.

At the vapor state, the slip length, L_s, can be evaluated by[10,18]

$$L_s = \lambda (2 - \alpha_v) / \alpha_v, \quad (1)$$

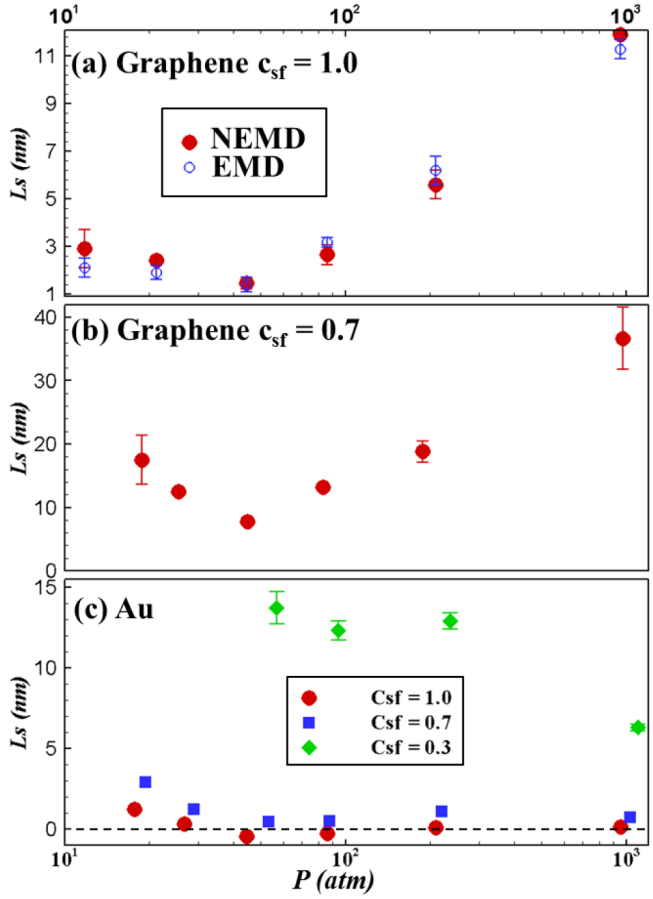

FIG. 3. Slip length as a function of pressure on (a) a graphene surface with $c_{sf} = 1.0$; (b) a graphene surface with $c_{sf} = 0.7$; (c) a Au surface with $c_{sf} = 1.0$, 0.7 and 0.3.

where λ is the molecular MFP and α_v is the momentum accommodation coefficient of vapor molecules on graphene. As vapor pressure increases, the adsorption coverage of fluid molecules on graphene increases, which leads to the increase of α_v.[19] Meanwhile, λ decreases with increasing pressure. Therefore, according to Eq. (1), the decrease of slip length with increasing pressure at the vapor state is expected, which is consistent with our results in the low-pressure regime. Above P_{cr}, the fluid is at the supercritical state and the slip length increases with increasing pressure as shown in Fig. 3(a).

D. EMD determination of slip length on graphene

To understand the increase of slip length with increasing pressure in the supercritical region, we carry out EMD simulations and calculate the slip length using the relation $L_s = \eta/\kappa$, where η is the fluid viscosity and κ is the Navier friction coefficient.[20] For Newtonian fluids, the shear stress is proportional to η and the shear stress exerted on the solid surface is by definition proportional to κ.[3,20] Since the shear stress has to be the same within the fluid and at the interface, the slip boundary condition is defined via $\kappa v_s = \eta(dv_x/dz)|_{wall}$, where v_s is the slip velocity. From this and the slip length definition, it follows that $L_s = \eta/\kappa$. The fact that the slip length is proportional to the viscosity can be intuitively understood via following. The slip length is the thickness of the fluid over which the velocity change is the same as the velocity discontinuity at the interface. Since, at a given shear stress, the velocity gradient is inversely proportional to the viscosity, the slip length is proportional to the viscosity.

The friction coefficient κ can be determined by the Green-Kubo relation for the force autocorrelation function[21,22]

$$\kappa = \frac{1}{Ak_BT}\int_0^\infty dt\,\langle F_x(t)\,F_x(0)\rangle\,, \qquad (2)$$

where k_B is the Boltzmann constant and F_x is the force acting on the solid by the fluid in the x-direction (in plane). In EMD simulation, both upper and lower walls are stationary by fixing the position of atoms in the outer planes of two graphene walls, and data from 10 ns runs are used to evaluate the correlation function of force.

Fig. 4(a) shows the force autocorrelation function and its running integral for the fluid at the highest simulated pressure. The friction coefficient κ is obtained from the plateau of the running integral. Similarly, the viscosity η can be obtained from the running integral of the shear-stress correlation function in a bulk fluid.[23,24] Fig. 3(a) shows that the slip length predicted by EMD simulations has a good agreement with those from NEMD simulations.

The EMD results show that from $P_{cr} = 44$ atm to $P = 955$ atm, the viscosity η increases ~10 times and the friction coefficient κ increases by 65%. This is illustrated in Fig. 4(b) and it clearly demonstrates that the increase of slip length with increasing pressure in the supercritical region is due to the fact that the viscosity of the fluid increases much faster with pressure than does the friction coefficient.

To further understand the variation of the friction coefficient with pressure in the supercritical region, we analyze our

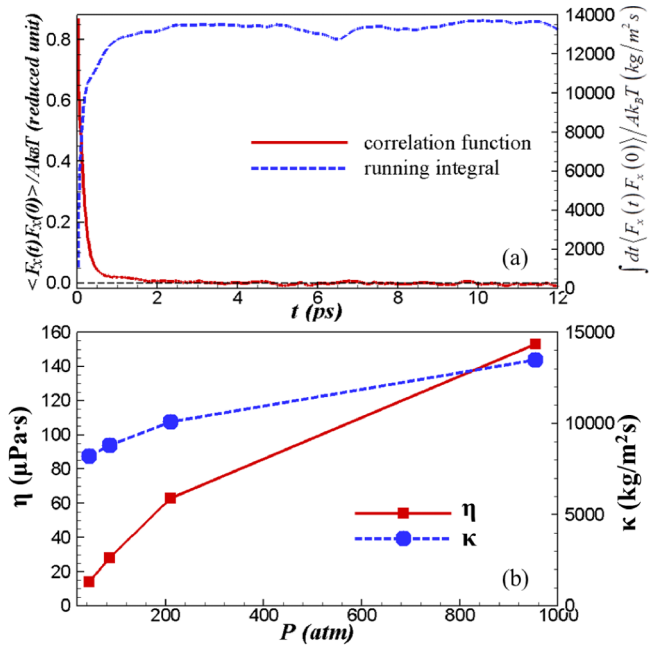

FIG. 4. (a) EMD simulation results of the autocorrelation function of shear force between graphene and fluid Ar and the running integral of the force correlation function. The simulation is performed at 150 K and 955 atm. (b) The viscosity η and friction coefficient κ as a function of pressure. The uncertainty is smaller than the symbol size. The lines are used to guide the eye.

results using the approximate relationship[25,26]

$$\kappa \simeq \frac{S_{\parallel}(q_0)}{2D_{\parallel}k_BT}\int_0^{\infty} dz\rho(z)V_1^2(z). \quad (3)$$

Equation (3) demonstrates the role of various microscopic factors affecting the friction coefficient. In particular, $\rho(z)$ is the fluid density profile near the wall and q_0 is the first reciprocal lattice vector of the graphene plane crystal structure in the flow direction. On a graphene surface, $q_0 = 2\pi/a$, where $a = 4.26$ Å is the lattice constant of graphene in the x-direction. $S_{\parallel}(q_0)$ and $D_{\parallel}$ are the structure factor and the collective diffusion coefficient that measure the fluid response to the corrugated potential of the surface.

$S_{\parallel}(q_0)$ and $D_{\parallel}$ are computed from the correlations of density fluctuations in the first fluid layer near the wall,[25,26]

$$S_{\parallel}(q_0,t) = \frac{\left\langle \rho^*_{q_0}(t)\,\rho_{q_0}(0)\right\rangle}{N} = S_{\parallel}(q_0)\,e^{-q_0^2 D_{\parallel} t}, \quad (4)$$

where $\rho_{q_0}(t) = \sum_{j=1}^{N} e^{iq_0x_j(t)}$ is a summation over all fluid atoms in the first layer and N is the average number of fluid atoms in the first layer. We define the fluid region less than $\sigma_{Ar\text{-}Ar}$ away from the surface as the first fluid layer. At each state point, EMD runs are carried out for 200 ps to determine the density correlation function. Fig. 5(a) shows the density correlation function of fluid Ar on graphene at the highest simulated pressure (955 atm). The correlation function in Fig. 5(a) exhibits an exponential decay with time as expected. The value of $S_{\parallel}(q_0,t)$ at $t = 0$ gives $S_{\parallel}(q_0) = 0.44$. An exponential fit to the initial 2.5 ps gives $q_0^2 D_{\parallel} = 1.05\ \text{ps}^{-1}$, thus $D_{\parallel} = 4.82 \times 10^{-9}\ \text{m}^2/\text{s}$.

Another quantity to be evaluated in Eq. (3) is $V_1(z)$, the amplitude of variation of solid-fluid interaction potential at a given z-plane. To determine $V_1(z)$ at each z-plane, we calculate

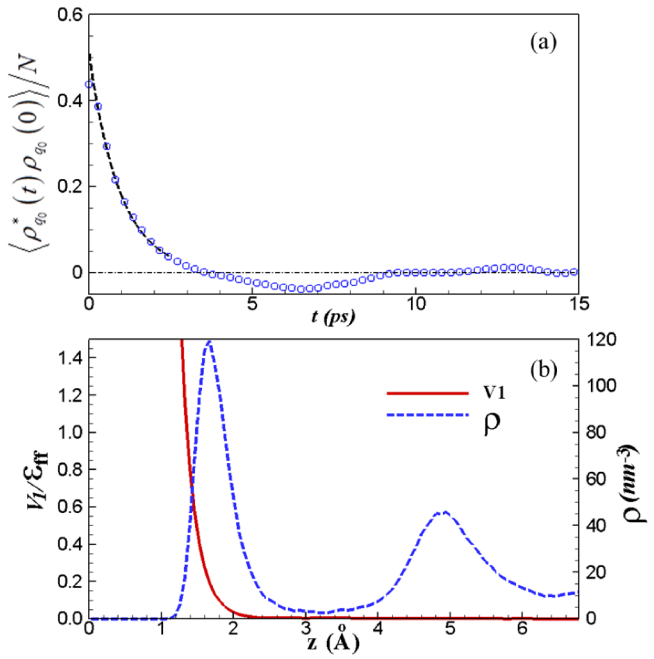

FIG. 5. (a) The density correlation function of fluid in the first layer near the graphene at 955 atm, and (b) the density distribution ρ(z) and V_1 near graphene surface at 955 atm.

the solid-fluid interaction potential as a function of x and y coordinates and find the maximum potential, $V_{max}(z)$, and the minimum potential, $V_{min}(z)$. $V_1(z)$ is computed by $(V_{max}(z) - V_{min}(z))/2$. Fig. 5(b) shows the fluid density distribution $\rho(z)$ and $V_1(z)$ near the graphene surface at the highest simulated pressure. The same method is applied to calculate $S_{\parallel}(q_0)$, $D_{\parallel}$, $\rho(z)$, and $V_1(z)$ at lower pressures. The simulation results are summarized in Table I.

As the pressure increases from 44 atm to 955 atm, Table I results show that $S_{\parallel}(q_0)/D_{\parallel}$ is essentially pressure independent, while the integral $\int dz\rho(z)V_1^2(z)$ is almost doubled. The results from Eq. (3) indicate that the increase of friction coefficient with increasing pressure is mainly due to the stronger layering of fluid (increase of $\rho(z)$) near the wall at higher pressures. At the same time, however, the viscosity increases by a factor of ten, leading to an overall slip length increase.

From Table I, we can see that the theoretical model based on Eq. (3), which is a simple approximation of Eq. (2), predicts a reasonable trend of slip length as a function of increasing pressure and provides a fundamental understanding of the slip length crossover on graphene. However, it cannot be used for quantitative predictions of slip length.

E. Slip length on Au as a comparison

To place the slip length pressure dependence on graphene in perspective, we carry out similar MD simulations of slip flow in a Au nanochannel. Each Au wall is formed by a three-layered FCC (100) plane solid Au with a cross section area of 5.3 nm × 5.3 nm. The embedded-atom-method (EAM) potential[27] is used for Au-Au interactions. The LJ potential, which is widely used for non-bonded interactions between fluid and solid surfaces,[3,6,28–30] is employed for Au-Ar interactions. The interaction parameters are the same as those for Ar-Ar interactions. All other settings are the same as those in the simulation of slip flow on graphene.

The velocity profile of a Couette flow in the Au channel at the highest simulated pressure is shown in Fig. 1(c). The result shows the slip length is essentially zero. The NEMD simulation results of slip length on Au as a function of pressure are shown in Fig. 3(c). In the vapor state, the slip length on Au decreases with increasing pressure as expected. In the supercritical state, however, no evident increase of slip length with pressure is observed.

To understand this behavior, we again turn to Eq. (3). The EMD simulation results which are summarized in Table II show that from 44 atm to 955 atm, $S_{\parallel}(q_0)/D_{\parallel}$ increases by 29%, the integral $\int dz\rho(z)V_1^2(z)$ increases by 128%, and accordingly, the friction coefficient κ is almost tripled on a Au surface. As the viscosity of fluid η increases much faster with the increasing pressure than the friction coefficient κ in the simulated supercritical states, the relation $L_s = \eta/\kappa$ predicts an increase of slip length by a factor of 4. Such an increase is not evident in Fig. 3(c) because the surface density of Au is much smaller than graphene, which leads to a significantly larger surface potential corrugation[1,3] and negligible slip lengths.

Fig. 6 shows the variation of solid-fluid interaction potential measured at a z-plane located at the position of the first peak of fluid density near the wall. According to Fig. 6, the

TABLE I. The simulation results as a function of pressure. ρ in the second column represents the density of fluid at the center of the channel. $L_{s,th}$ is the slip length obtained using the friction coefficient calculated by Eq. (3) in the paper.

P (atm)	ρ (nm^{-3})	η (μPa s)	$S_{\|}(q_0)$	$D_{\|}$ (m^2/s)	$\int dz\rho V_1^2$ (J^2/m^2)	$L_{s,th}$ (nm)	$L_{s,NEMD}$ (nm)
44.5	3.24	14	0.71	8.4×10^{-9}	1.25×10^{-24}	0.55	1.5 ± 0.25
86.1	8.48	28	0.77	6.8×10^{-9}	1.55×10^{-24}	0.66	2.6 ± 0.41
210.1	14.25	63	0.62	6.8×10^{-9}	1.64×10^{-24}	1.74	5.6 ± 0.60
954.5	19.47	153	0.44	4.8×10^{-9}	2.46×10^{-24}	2.81	11.9 ± 0.20

TABLE II. Same as Table I except that these are the simulation results for fluid Ar on Au.

P (atm)	ρ (nm^{-3})	η (μPa s)	$S_{\|}(q_0)$	$D_{\|}$ (m^2/s)	$\int dz\rho V_1^2$ (J^2/m^2)	$L_{s,th}$ (nm)	$L_{s,NEMD}$ (nm)
44.5	3.24	14	1.42	5.1×10^{-9}	2.97×10^{-22}	0.0007	−0.45 ± 0.20
86.1	8.48	28	1.44	4.1×10^{-9}	3.30×10^{-22}	0.0010	−0.25 ± 0.10
210.1	14.25	63	1.44	3.3×10^{-9}	3.98×10^{-22}	0.0015	0.10 ± 0.10
954.5	19.47	153	1.11	3.1×10^{-9}	6.80×10^{-22}	0.0026	0.13 ± 0.10

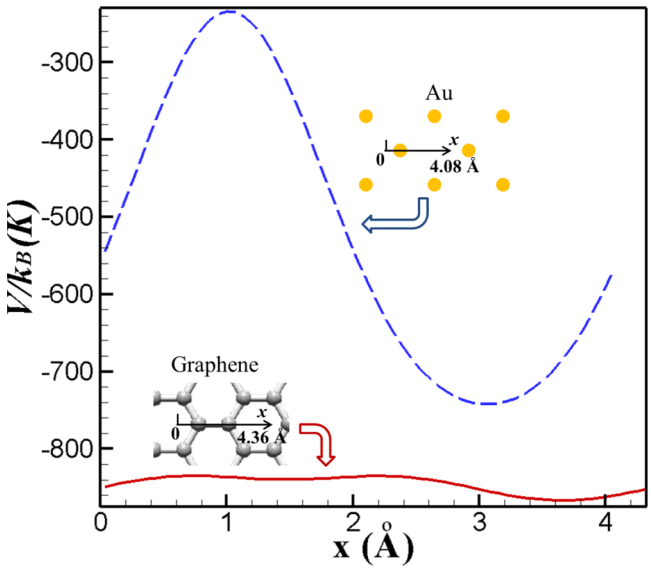

FIG. 6. The surface potential distribution in the x-direction (flow direction) on a graphene surface and a Au surface. The surface potential is obtained in a z-plane located at the position of first density peak of fluid near the wall. The two potential distributions shown in the figure are obtained along the lines indicated in the two insets.

amplitude of the potential variation, V_1, on a Au surface is more than 10 times greater than that on a graphene surface. According to Eq. (3), the much greater V_1 on Au surface leads to a significantly larger friction coefficient, and thus essentially zero slip length is obtained at all the simulated supercritical states. It is shown in Table II that the L_s from NEMD simulations is comparable to the magnitude of its uncertainty, which makes increase of L_s with pressure not evident.

To observe a clear pressure dependence of the slip length on Au, we reduce the coarseness of the potential surface on Au by multiplying the attractive part of the LJ potential for solid-fluid interactions by a factor C_{sf}. For $C_{sf} = 0.7$, the slip length at all the simulated states is enhanced as shown in Fig. 3(c). In the supercritical region, however, the slip lengths are still too small to see a clear pressure dependence. As a comparison, we also set $C_{sf} = 0.7$ for solid-fluid interactions on graphene. It is shown in Fig. 3(b) that the slip length of fluid Ar on graphene is significantly enhanced and the minimum slip length is still obtained at the pressure close to P_{cr}.

To see an evident slip of flow on Au, we further reduce C_{sf} for Au-Ar interactions to 0.3. The NEMD simulation results in Fig. 3(c) show that the slip length essentially goes down with increasing pressure in the supercritical region. For $C_{sf} = 0.3$, the solid-fluid attraction force is extremely small, which leads to a strong density depletion near the wall at low pressures. At the highest simulated pressure, a strong layering of fluid at the wall is observed. Similar phenomena were also observed in previous MD simulations.[11] The significant difference in $\rho(z)$ makes the integral $\int dz\rho(z)V_1^2(z)$ increase by a factor of 22 from the lowest pressure to the highest pressure in the simulated supercritical states. For $C_{sf} = 0.3$, therefore, the friction coefficient κ increases faster with increasing pressure than the viscosity η, which results in a decrease of slip length with increasing pressure.

III. SUMMARY AND CONCLUSIONS

In summary, we studied the dependence of the slip length of supercritical argon fluid on graphene as a function of pressure. Using both equilibrium and non-equilibrium molecular dynamics simulations, we found, consistently, that the slip length first decreases with increasing pressure at the vapor state due to the reduced mean free path of vapor molecules, and then increases with increasing pressure because the viscosity of fluid increases much faster with increasing pressure than the friction coefficient. The minimum slip length is obtained at the pressure close to the critical pressure, when the structure of the fluid transitions from gas to liquid-like, which coincides with an onset of a rapid fluid viscosity increase with increasing pressure.

Although the presence of the minimum slip length is quite general, however, on most surfaces at the high pressure regime, the slip length is very small, and from a practical consideration, it is equal to zero (no-slip boundary conditions). We demonstrated that this is the case even for an atomistically smooth gold surface. The high atomic surface density of graphene

leads to a very smooth energy landscape associated in-plane slip. Therefore, in this case, the surface friction is very low and weakly pressure dependent. These characteristics expose the role of increasing fluid viscosity at high pressures leading to a significant slip length increase.

ACKNOWLEDGMENTS

This work greatly benefited from a discussion and advice from Professor J.-L. Barrat. This work is supported by the U.S. Air Force Office of Scientific Research Grant No. FA9550-12-1-0351. We would like to thank eXtreme Science and Engineering Discovery Environment (XSEDE) for providing us supercomputer resources for MD simulations.

[1]P. A. Thompson and S. M. Troian, Nature **389**, 360 (1997).
[2]Y. Ren and D. Stein, Nanotechnology **19**, 195707 (2008).
[3]S. K. Kannam, B. D. Todd, J. S. Hansen, and P. J. Daivis, J. Chem. Phys. **135**, 144701 (2011).
[4]A. Maali, T. C. Bouhacina, and H. Kellay, Appl. Phys. Lett. **92**, 053101 (2008).
[5]X. Qin, Q. Yuan, Y. Zhao, S. Xie, and Z. Liu, Nano Lett. **11**, 2173 (2011).
[6]S. K. Kannam, B. D. Todd, J. S. Hansen, and P. J. Daivis, J. Chem. Phys. **136**, 024705 (2012).
[7]W. Xiong, J. Z. Liu, M. Ma, Z. Xu, J. Sheridan, and Q. Zheng, Phys. Rev. E **84**, 056329 (2011).
[8]J. A. Thomas and A. J. H. McGaughey, Nano Lett. **8**, 2788 (2008).
[9]K. Falk, F. Sedlmeier, L. Joly, R. R. Netz, and L. Bocquet, Nano Lett. **10**, 4067 (2010).
[10]F. O. Goodman and H. Y. Wachman, *Dynamics of Gas-Surface Scattering* (Academic Press, New York, 1976), pp. 23-31.
[11]J.-L. Barrat and L. Bocquet, Phys. Rev. Lett. **82**, 4671 (1999).
[12]L. Lindsay and D. A. Broido, Phys. Rev. B **81**, 205441 (2010).
[13]L. A. Girifalco, M. Hodak, and R. S. Lee, Phys. Rev. B **62**, 13104 (2000).
[14]G. C. Maitland, M. Rigby, E. B. Smith, and W. A. Wakeham, *Intermolecular Forces: Their Origin and Determination* (Clarendon Press, Oxford, 1981).
[15]D. Frenkel and B. Smit, *Understanding Molecular Simulation* (Academic Press, San Diego, 2002), p. 426.
[16]Z. Liang, K. Sasikumar, and P. Keblinski, Phys. Rev. Lett. **111**, 225701 (2013).
[17]H. J. C. Berendsen, J. P. M. Postma, W. F. Van Gunsteren, A. Di Nola, and J. R. Haak, J. Chem. Phys. **81**, 3684 (1984).
[18]J. C. Maxwell, Philos. Trans. R. Soc. London **170**(Pt. 1), 231 (1879).
[19]Z. Liang and P. Keblinski, Int. J. Heat Mass Transfer **78**, 161 (2014).
[20]C. L. M. H. Navier, Mem. Acad. Sci. Inst. Fr. **6**, 389 (1823).
[21]L. Bocquet and J.-L. Barrat, Phys. Rev. E **49**, 3079 (1994).
[22]L. Bocquet and J.-L. Barrat, J. Chem. Phys. **139**, 044704 (2013).
[23]Z. Liang and H.-L. Tsai, Fluid Phase Equilib. **293**, 196 (2010).
[24]Z. Liang and H.-L. Tsai, Mol. Phys. **108**, 1285 (2010).
[25]J.-L. Barrat and L. Bocquet, Faraday Discuss. **112**, 119 (1999).
[26]L. Bocquet and J.-L. Barrat, Soft Matter **3**, 685 (2007).
[27]S. M. Foiles, M. I. Baskes, and M. S. Daw, Phys. Rev. B **33**, 7983 (1986).
[28]Z. Liang and H.-L. Tsai, Phys. Rev. E **83**, 061603 (2011).
[29]Z. Liang, W. Evans, and P. Keblinski, Phys. Rev. E **87**, 022119 (2013).
[30]Z. Liang, W. Evans, T. Desai, and P. Keblinski, Appl. Phys. Lett. **102**, 061907 (2013).